Noname manuscript No.
(will be inserted by the editor)

Carlos Simão Ferreira · Fulvio Scarano · Gijs van Kuik · Gerard van Bussel

Aerodynamic Force on a VAWT in Dynamic Stall by Integration of the Velocity Field from 3C Particle Image Velocimetry

Received: date / Accepted: date

Abstract The paper focuses on evaluating the feasibility of estimating loads on Vertical Axis Wind Turbine (VAWT) blades in dynamic stall by velocity data acquired with Particle Image Velocimetry (PIV). The work uses simulated velocity data from a Detached Eddy Simulation (DES) at space and time refinement equivalent to that obtained with PIV, thus estimating error associated. This research is part of a five step research on estimating loads on small VAWT integrated in the Urban Wind Energy research in DUWIND - Delft University Wind Energy Research Institute.

Nomenclature

V	Control volume
c	airfoil/blade chord, m
C_N	normal force coefficient
C_T	tangential force coefficient
D	rotor diameter, m
F	aerodynamic force, N
k	reduced frequency
p	static pressure, Pa
p_∞	static pressure at infinity, Pa
k	reduced frequency
R	rotor radius, m
S	Outer contour of control volume
S_b	Inner contour of control volume
t	time
T	stress tensor, m^2/s^2
u	local velocity, m/s
U_∞	Unperturbed velocity, m/s
α	angle of attack
λ	tip speed ratio $\Omega_{Rot}.R/U_\infty$
θ	azimuth angle
ρ	fluid density kg/m^3
ω	perturbation frequency, rad/s
Ω	vorticity, s^{-1}
Ω_{Rot}	angular velocity of rotor, rad/s
μ	dynamic viscosity

All authors
Kluyverweg 1, 2629 HS, Delft, The Netherlands
Tel.: +31 15 278 20 73 (corresponding author)
Fax: +31 15 278 53 47
E-mail: c.j.simaoferreira@tudelft.nl

1 Introduction

The development of wind turbine aerodynamics requires extensive wind tunnel experimental research, not only to identify and understand physical processes but also to validate numerical models and quantify performance. Wind tunnel research is usually limited by its cost and mainly by the inability to correctly simulate real conditions (Reynolds number, reduced frequency, tip speed ratio) due to wind tunnel size and power.

Another constraint is the limited access to the flow or the inability/complexity of measuring certain flow properties. Currently, most experimental results on rotors are usually confined to pressure measurements over the surface and wake measurements of velocity or wake location.

The latest years have seen an increase of the application of Particle Image Velocimetry (PIV) to rotor aerodynamics, mainly in the characterization of the flow field in the wake of the rotor. The current research aims at using 2D and 3C PIV (three velocity component PIV, a.k.a Stereo PIV) to determine the force over the blades of a Vertical Axis Wind Turbine (VAWT) in dynamic stall.

The theoretical evaluation of the momentum equation to determine the body force from velocity field data has been thoroughly developed (see Noca [1]). Current research by the authors aims at applying the theory to the unsteady flow of a VAWT in dynamic stall, identifying and developing the procedure to implement the method to PIV measurements.

2 Methodology

The research methodology is divided in five main parts, of which this is the third. The first part consisted on the eval-

uation of the 2D flow field of a VAWT in dynamic stall a low tip speed ratios (large angles of attack), which was conducted in the work of Simão Ferreira et al [4]. The visualization and quantification of the flow field in terms of the development of the shed vorticity and wake was used for the validation of the second part of the research, the development of a 2D Navier-Stokes model of the VAWT in dynamic stall (see Simão Ferreira et al [2] and [3]).

Several turbulence models where tested for the *2D Navier-Stokes* simulation, with the most accurate results obtained with a *DES* (*Detached Eddy Simulation*). The simulation managed to replicate the vorticity shedding process and wake development, both in phase and in magnitude.

The third and current part of the research methodology aims at using the velocity data from the *2D Navier-Stokes* simulation to test the feasibility of estimating the loads on a VAWT airfoil in dynamic stall using only the velocity data, as it would result from PIV measurements. The results are compared with the force data obtained in the simulation and a sensitivity analysis to time and space grid refinement is performed.

The future fourth and fifth parts of the research involve the application of the procedure to real experimental velocity data.

3 The 2D Navier-Stokes simulation

The geometry of the model is a 2D representation of the experimental setup of Simão Ferreira et al [4]. The model's wall boundary conditions consists of two walls spaced $1.25m$ apart, where a $0.4m$ diameter single-bladed Darrieus VAWT is placed. The rotor is represented by an $0.05m$ chord *NACA0015* airfoil and the $0.05m$ rotor axis. The rotor axis is placed over the symmetry position of the wind tunnel. The inlet and outlet boundary conditions are placed respectively $10D$ upwind and $14D$ downwind of the rotor, allowing a full development of the wake.

The model includes a 2D spatial grid, simulating the conditions at the middle cross-section of the experimental setup. The grid is composed of four non-conformal sub-grids, each a structured grid of quadrilateral elements. Figure 3 presents a diagram of the shape and location of each sub-grid and the wall boundary conditions representing the airfoil/blade, wind tunnel walls and rotor axis (the flow inlet and outlet boundary conditions are not represented).

The use of moving sub-grids is necessary due to the movement of the rotor elements. Thus, the sub-grids *Rotor Diameter*, *Blade sub-grid I*, and *Blade sub-grid II* rotate with an angular velocity $\omega = 75rad/s$, while the sub-grid *Wind Tunnel* remains fixed. The grid comprises 3305 nodes over the airfoil surface, where the height of the first row of cells is set at a distance to the wall of $0.02\%c$ to ($y^+ \approx 1$ when $\theta = 90°$, $k-\varepsilon$ model). The total model size comprises approx. $1.6 * 10^6$ cells.

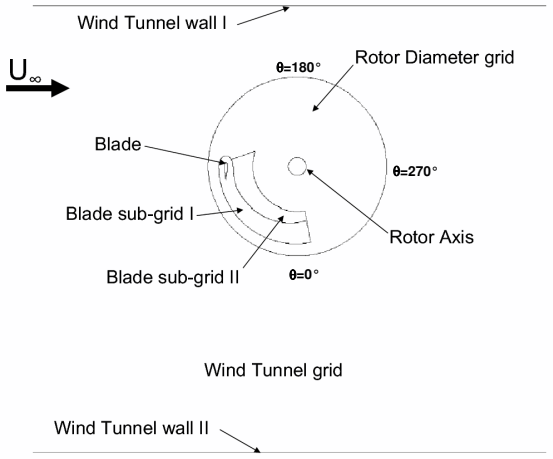

Fig. 1 Diagram of the model geometry, sub-grid distribution and boundary conditions.

3.1 Simulated flow conditions

The simulation aimed at representing the flow conditions of the experimental work for $\lambda = 2$ and incoming flow $U_\infty = 7.5m/s$. The level of unsteadiness is determined by the reduced frequency k, defined as $k = \omega \cdot c/2V$, where ω is the angular frequency of the unsteadiness, c is the blade's chord and V is the velocity of the blade. In this experiment, due to the variation of V with rotation angle, k was defined as $k = \omega \cdot c/(2\lambda \cdot V_\infty) = \omega \cdot c/(2\omega \cdot R) = c/(2R)$, where λ is the tip speed ratio and R is the radius of rotation. For this experimental work $k = 0.125$, placing the work in the unsteady aerodynamics region.

Due to the importance of the induction of the rotor, it is necessary to perform a simulation for several rotations until a fully developed wake is present. All values presented in this paper relate to the revolutions of the rotor after a periodic post-transient solution is found.

4 Theoretical background

Consider a time-dependent control volume applied in a viscous unsteady flow, comprising a volume V [1] that is bounded by two surfaces S and S_B, as depicted in Figure 3. The fluid dynamic force per unit density F/ρ acting on the body can be expressed by Equation 1.

$$\begin{aligned}\frac{F}{\rho} = &-\frac{d}{dt}\int_{V_{(t)}} \mathrm{u}\,dV \\ &+ \oint_{S_{(t)}} \hat{\mathrm{n}} \cdot \left[-\frac{p}{\rho}\mathrm{I} - (\mathrm{u}-\mathrm{u_S})\,\mathrm{u} + \mathrm{T}\right] dS \\ &- \oint_{S_{b(t)}} \hat{\mathrm{n}} \cdot \left[(\mathrm{u}-\mathrm{u_S})\,\mathrm{u}\right] dS\end{aligned} \tag{1}$$

where T is the viscous stress tensor

$$T = \mu\left(\nabla \mathrm{u} + \nabla \mathrm{u}^{\mathrm{T}}\right) \tag{2}$$

[1] The notation presented by Noca et al [1] will be used for most of this work.

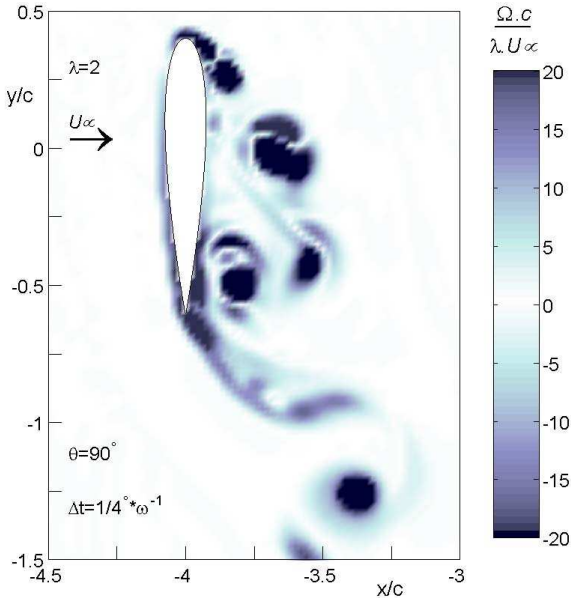

Fig. 2 Vorticity field at $\theta = 90^\circ$, *Detached Eddy Simulation*.

The determination of fluid forces by the application of Equation 1 with PIV and other experimental data presents two main challenges:

1. the equation requires the determination of the velocity in the entire control volume; this is mostly unfeasible due to the difficulty of measuring in the boundary layer regions;
2. the equation requires the determination of the pressure over the outside contour of the control volume;

Noca et al [1] proposes a different formulation o the momentum balance: *the Flux Equation* (Equation 3)

$$\begin{aligned}\frac{F}{\rho} = &+\oint_{S_{(t)}} \hat{\mathrm{n}}\cdot\gamma_{\mathrm{flux}}\,dS \\ &-\oint_{S_{b(t)}} \hat{\mathrm{n}}\cdot[(\mathrm{u}-\mathrm{u_S})\,\mathrm{u}]\,dS - \frac{d}{dt}\oint_{S_{b(t)}} \hat{\mathrm{n}}\cdot(\mathrm{ux})\,dS\end{aligned} \tag{3}$$

with the *flux term* γ_{flux}

$$\begin{aligned}\gamma_{\mathrm{flux}} = &\tfrac{1}{2}\mathrm{u}^2\mathrm{I} - \mathrm{uu} - \tfrac{1}{N-1}\mathrm{u}\,(\mathrm{x}\times\boldsymbol{\omega}) + \tfrac{1}{N-1}\boldsymbol{\omega}\,(\mathrm{x}\times\mathrm{u}) \\ &-\tfrac{1}{N-1}\left[\left(\mathrm{x}\cdot\tfrac{\partial \mathrm{u}}{\partial t}\right)\mathrm{I} - \mathrm{x}\tfrac{\partial \mathrm{u}}{\partial t} + (N-1)\,\tfrac{\partial \mathrm{u}}{\partial t}\mathrm{x}\right] \\ &+\tfrac{1}{N-1}\left[\mathrm{x}\cdot(\nabla\cdot\mathrm{T})\,\mathrm{I} - \mathrm{x}\,(\nabla\cdot\mathrm{T})\right] + \mathrm{T}\end{aligned} \tag{4}$$

The flux equation require only terms of velocity and its derivatives over the boundaries of the control volume. For a 2D body with a solid wall S_b, this problems simplifies to determining the velocities and its time derivatives in the region of the outside contour S.

Yet, the elimination of the pressure term implies the appearance of the explicit formulation of the vorticity term $\boldsymbol{\omega}$. For the case of large wakes (bluff body flows) and good description of the velocity field on the wake, the *Flux Equation* is an efficient method to determine the loads on the body. For thin boundary layer, the relative coarseness of the measurement data can be a source of error. The asymptotic variation

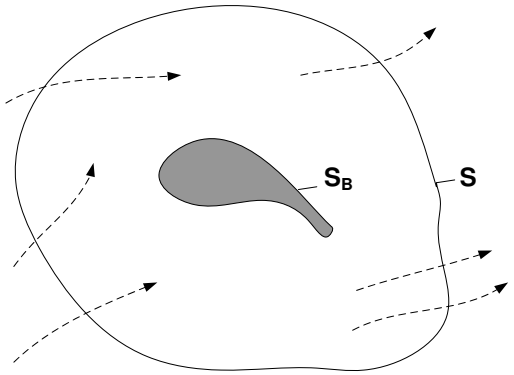

Fig. 3 Representation of the control volume bounded by the outer contour S and the body contour S_B

of vorticity over the contour as it crosses the wake can result in a significant numerical integration error; also, the averaging of the flow field due to the size of the interrogation window in the PIV processing can lead to an experimental measurement error/bias. This difficulty can be overcome by a change of reference frame where the origin is set at the wake, thus reducing the influence of the vorticity term at the wake.

A robust formulation to overcome the insufficient refinement of data at the wake is to explicitly express the pressure term (Equation 5).

$$\gamma_{\mathrm{flux}} = \tfrac{\mathrm{p}}{\rho}\mathrm{I} - \mathrm{uu} - \tfrac{\partial \mathrm{u}}{\partial t}\mathrm{x} + \mathrm{T} \tag{5}$$

The disadvantage of this method is that it requires the estimation of the gradient of the pressure along the contour, once again coming across the problem of integration of a velocity gradient across the wake (Equation 6).

$$-\nabla\tfrac{\mathrm{p}}{\rho} = -\tfrac{\partial \mathrm{u}}{\partial t} + (\mathrm{u}\cdot\nabla)\,\mathrm{u} - \nabla\cdot\mathrm{T} \tag{6}$$

The error of estimation of the pressure gradient across the wake can be considered of little importance if the closed path of the pressure integration is set such that it starts and ends in the vicinity of the wake.

5 Validation of the calculation of the pressure gradient

The accuracy of the estimation of the pressure can be evaluated in Figure 4; the figure presents the value of pressure (made non-dimensional) calculated by the 2D Navier-Stokes simulation and the pressure estimated by integration of the velocity field obtained from the simulation.

As seen in Figure 4, the effect of the error on the estimation of the pressure gradient at the location where the contour crosses the wake is local; notice that the pressure estimated from the velocity data is not the actual pressure,

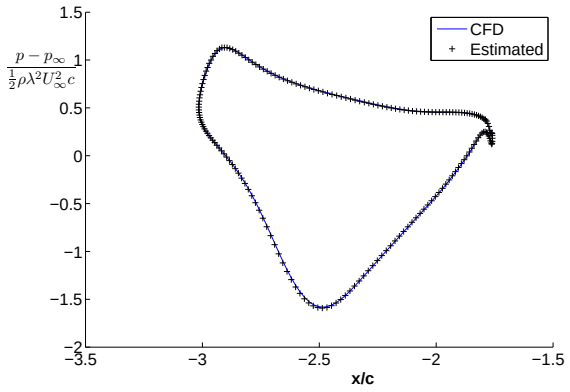

Fig. 4 Pressure result from CFD simulation and estimated (integration of the velocity data) over contour *B*(Figure 5).

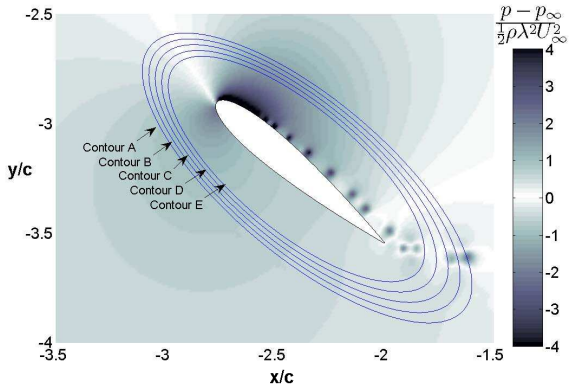

Fig. 5 Location of volume contours *A*,*B*,*C* and *D*. Results of the integration of the forces around these contours are presented in Table 6.

but a value at a difference of a reference constant. For calculation of the force term, only the variation of the pressure is relevant. The absolute value of pressure can be estimated by integration of the gradient from the far-field.

6 Comparison of the different formulations of the Flux Equation

In Table 6 the values of estimated *Normal Force Coefficient* $C_{N_{est}}$ and *Tangential Force Coefficient* $C_{T_{est}}$ are presented for different control volumes, defined by five different outer contours as presented in Figure 5. The results allow for two conclusions:

- the formulation with the explicit *Pressure* term (Equation 5) is less sensitive to the location of the contour than the conventional *Flux* formulation, especially the across the wake,
- the results for the *Pressure* formulation stand at an maximum difference of 5% for C_N and 10% for C_T to the 2D Navier-Stokes (CFD) calculated value.

	C_T		C_N	
	Flux	Pressure	Flux	Pressure
Contour A	-0.31	-0.28	2.62	2.65
Contour B	-0.27	-0.28	2.63	2.63
Contour C	-0.25	-0.26	2.65	2.65
Contour D	-0.27	-0.28	2.63	2.62
Contour E	-0.28	-0.29	2.62	2.61
CFD	-0.29		2.72	

Table 1 Comparison of C_N and C_T calculated by the *Flux* and *Pressure* method over different contours (see Figure 5). *CFD* value is obtained directly from the CFD simulation from airfoil surface integration.

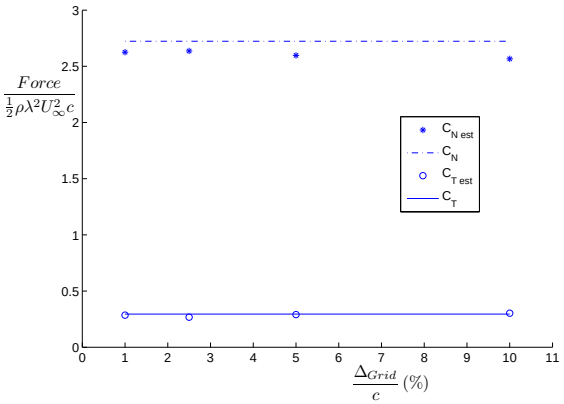

Fig. 6 Effect of the resolution of the velocity field Δ_{Grid}/c).Comparison of CFD results for normal and tangential force coefficient C_N and C_T and the estimates from integration of the velocity field C_{Nest} and C_{Test}.

The results show also that the result is largely insensitive to the choice of contour; this is under the condition that the contours avoid regions of large gradients.

7 Sensitivity to spatial grid resolution

One of the limitations for the accurate integration of the forces is the resolution of the velocity grid. Figure 6 presents the values estimated (*Pressure* formulation) for C_N and C_T for different resolutions of the space grid. The grid is a regular uniform grid, where the scale of the grid represents $\Delta x/c = \Delta y/c$. The estimates prove to be significantly robust even at very coarse grids.

8 Sensitivity to phase/time grid resolution

The high reduced frequency of the flow ($k = 0.125$) implies that the time dependent terms play an important role in the force estimation. The velocity time derivative terms are estimated by Equation 7

$$\frac{\partial \mathrm{u}}{\partial t} = \frac{\mathrm{u}_\theta - \mathrm{u}_{\theta+\Delta\theta}}{\Delta\theta/\omega} \tag{7}$$

Figure 7 shows the variation of force coefficients for different time refinements for calculation of the time deriva-

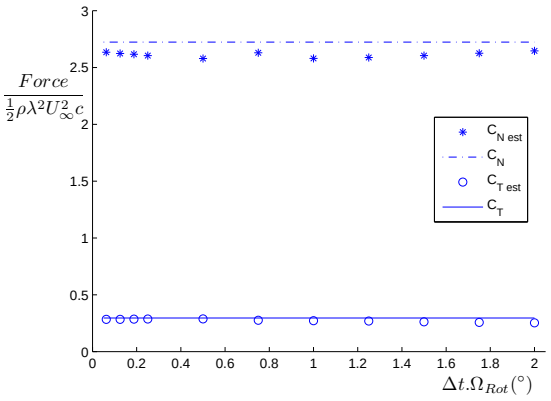

Fig. 7 Effect of the size of time/phase step Δt for estimation of the velocity time derivatives. Comparison of CFD results for normal and tangential force coefficient C_N and C_T and the estimates from integration of the velocity field C_{Nest} and C_{Test} for different sizes of Δt.

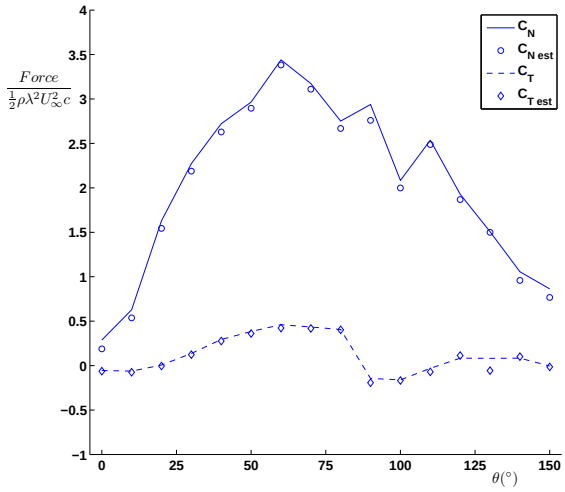

Fig. 8 Comparison of CFD results for normal and tangential force coefficient C_N and C_T and the estimates from integration of the velocity field C_{Nest} and C_{Test} for $\theta = 0$ to 150.

tives. The method shows little sensitivity to the error associated with the linear estimation of the time dependent terms.

9 Comparison along rotation

Figure 8 presents the evaluation of the forces estimated versus those given by the CFD model. The method is effective even at large azimuthal angles, in highly complex flow, under the presumption that the time dependent terms are correctly estimated.

10 Conclusions and future work

The estimation of loads on a VAWT airfoil undergoing dynamic stall by integration of the velocity data is proven feasible. The sensitivity analysis have shown that the method is robust to contour location, velocity data grid refinement and linear estimation of the velocity time derivative. The *Flux Equation* formulation from Noca et al [1] proved effective, as it did an explicit integration of the pressure term over the outer contour of the control volume. The integration across the wake requires a change of reference frame to overcome the influence of the error on estimating the strong velocity gradient. The method was validated over the development of dynamic stall from $\theta = 0^\circ$ to $\theta = 150^\circ$.

Further steps of the research will evaluate the effect of phase locked averaging of the flow field, flow field reconstruction and application to real PIV data.

References

1. Noca, F., Shiels, D., Jeon, D.: A comparison of methods for evaluating time-dependent fluid dynamic forces on bodies, using only velocity fields and their derivatives. Journal of Fluids and Structures **13**, 551–578 (1999)
2. Simão Ferreira, C., van Bussel, G., van Kuik, G.: 2d cfd simulation of dynamic stall on a vertical axis wind turbine: verification and validation with piv measurements. In: Abstract submited for the 2007 AIAA/ASME Wind Energy Symposium (2007)
3. Simão Ferreira, C., van Bussel, G., van Kuik, G., Bijl, H.: Simulating dynamic stall in a 2D VAWT: verification and validation with Particle Image Velocimetry data. In: The Science of Making Torque from Wind (2007)
4. Simão Ferreira, C., van Bussel, G., van Kuik, G., Scarano, F.: 2D PIV visualization of dynamic stall on a vertical axis wind turbine. In: 45^{th} AIAA Aerospace Sciences Meeting and Exhibit /ASME Wind Energy Symposium (2007)